_olin Swindells & Karon E. MacLean
Dept. of Computer Science, University of British Columbia
Tech Report: TR-2006-14, August 2006

Captured Dynamics Data of 5 Mechanical Knobs

Torque models are presented for five mechanical knobs that were characterized using the rotary haptic camera shown Figure 1. Non-linear least squares fitting was used to estimate model parameters for position, velocity, and acceleration model parts. Additionally, two simulated knobs were modeled to test the accuracy of the characterization algorithm.

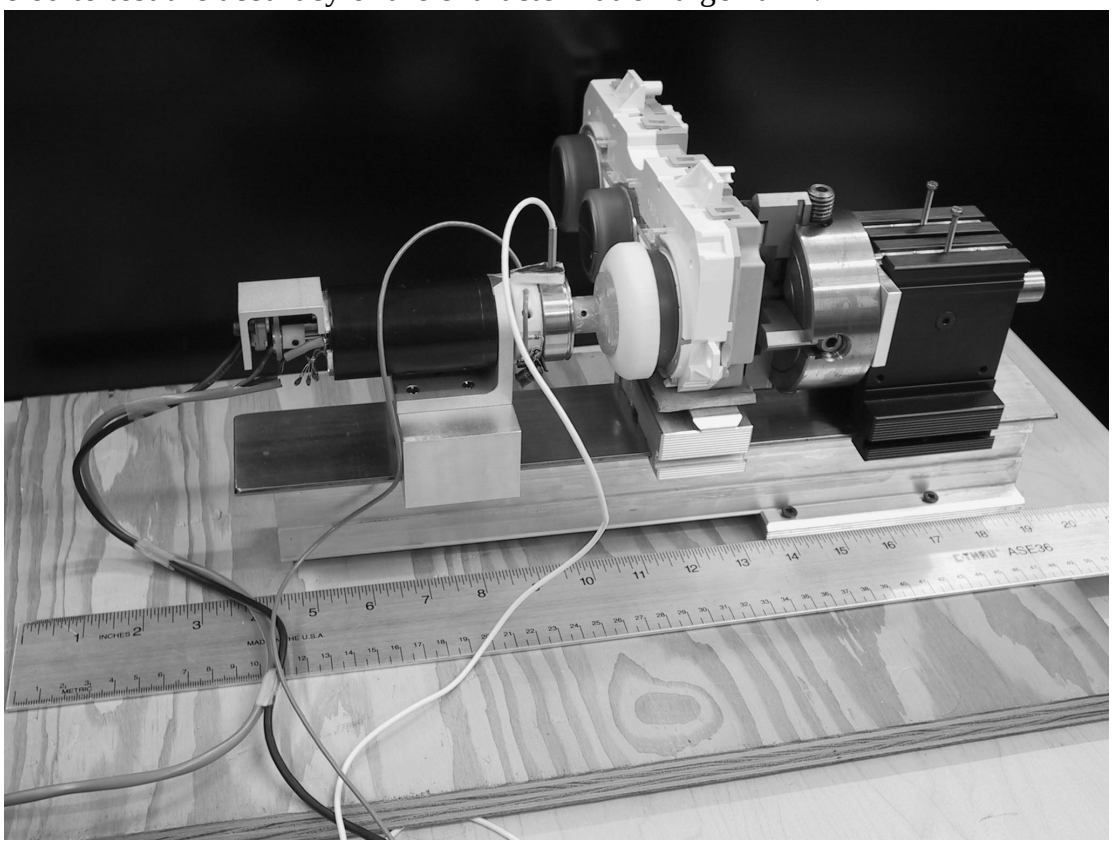

Figure 1: Rotary Haptic Camera Apparatus

1 Apparatus Summary

A haptic camera does for touch what a typical photographic camera does for vision. A typical visual camera measures the environment to build an image consisting of a 2D grid of coloured pixels. Likewise, a haptic camera

measures the *feel* of an environment and fits these measurements to a haptic model. The measured feeling can then be simulated by rendering the model on an appropriate haptic device. The haptic camera described in this document focuses on measurement of one kind of touch — kinaesthetic rotation about 1 axis (i.e., knobs). Physics-based dynamic models of friction and inertia 'store' the feel of an environment, and guide the rendering of feelings on a force-feedback knob. This haptic camera is an extension of similar mechanical property characterization devices such as those developed by MacLean [5], Colton & Hollerbach [1], and Richard [8].

Sensors were needed to measure angular position, velocity, acceleration, and torques. Table 1 lists resolutions for each of these quantities, and summaries of the different sensors are described below.

Table 1: Haptic camera sensor resolutions

Position	*Velocity*	*Acceleration*	*Torque*
9.8×10^{-6} rad	2.0×10^{-4} rad / s	2.8 rad / s^2	1.8×10^{-4} Nm

2 Knob Model

Torque responses to a knob's acceleration, velocity, and position were fit to a model using non-linear least-squares fitting. Non-linear (position) and linear (acceleration & velocity) parts were evaluated separately to improve fitting quality and speed. In other words, a Lur'e system of linear dynamic and non-linear static parts was assumed [2]. Matlab's "lsqcurvefit" and "\" commands were used to fit the non-linear and linear model parts, respectively [6]. Function minimization was forced to use the Levenberg-Marquardt method instead of the more traditional Gauss-Newton method because the Levenberg-Marquardt method has been shown to perform a better fit when using medium-scale problems like the ones presented in this thesis [3].

Equation 1 illustrates the system model used for both system identification and rendering of haptic knobs. Torque, position, velocity, and acceleration values are captured using the haptic camera, and then fit to the remaining

parameters in Equation 1. Refer to Figure 2 and Figure 3 for illustrations of the velocity and position functions that are annotated with the parameters of Equation 1.

$$\tau = \begin{cases} M_{acc}\ddot{\theta} & \text{acc. part } (\tau_{acc}) \\ C_{vel-}\operatorname{sgn}\dot{\theta}_{-} + B_{vel-}\dot{\theta}_{-} + C_{vel+}\operatorname{sgn}\dot{\theta}_{+} + B_{vel+}\dot{\theta}_{+} & \text{vel. part } (\tau_{vel}) \\ A_{pos}\sin\left(\frac{\theta}{P_{pos}} + S_{pos}\right) & \text{pos. part } (\tau_{pos}) \end{cases} \quad (1)$$

where

τ is the torque rendered to the force-feedback knob.

τ_{pos}, τ_{vel}, and τ_{acc} are the position, velocity, and acceleration torque parts that sum together to form τ.

θ, $\dot{\theta}$, and $\ddot{\theta}$ are the rotational position, velocity, and acceleration.

M_{acc} is an acceleration constant intuitively similar to inertia.

C_{vel-} and C_{vel+} are the negative and positive values of dynamic friction.

B_{vel-} and B_{vel+} are the negative and positive values of viscous friction.

A_{pos}, P_{pos}, and S_{pos} are a set of possible position parameters to render detents. Examples of other possible position functions include one or more ramps, $K_{pos}\theta$, or polynomials $P3_{pos}\theta^3 + P2_{pos}\theta^2 + P1_{pos}\theta + P0_{pos}$.

A_{pos}, P_{pos}, and S_{pos} change the amplitude, period, and phase shifts, respectively.

Equation 2 and Figure 2 illustrate a version of Karnopp's friction model used for characterization and rendering [4]. More sophisticated models such as the Stribeck effect could be used, but the practical ability to both capture and render subtleties in torque beyond the Karnopp model are beyond the scope of this document [9].

$$\tau_{friction} = \begin{cases} C_{vel-}\,\mathrm{sgn}\,\dot{\theta} + B_{vel-}\,\dot{\theta} & \text{for} \quad \dot{\theta} < -\Delta v \\ \max(C_{vel-},\ \tau_{other}) & \text{for} \quad -\Delta v < \dot{\theta} < 0 \\ \min(C_{vel+},\ \tau_{other}) & \text{for} \quad 0 < \dot{\theta} < \Delta v \\ C_{vel+}\,\mathrm{sgn}\,\dot{\theta} + B_{vel+}\,\dot{\theta} & \text{for} \quad \dot{\theta} > \Delta v \end{cases} \tag{2}$$

where

τ_{other} represents the non-frictional torque currently applied to the knob.

Δv, and below, are the values at which we assume the velocity to zero.

D_{vel-} and D_{vel+} are the negative and positive values of static friction.

The other constants are the same as above.

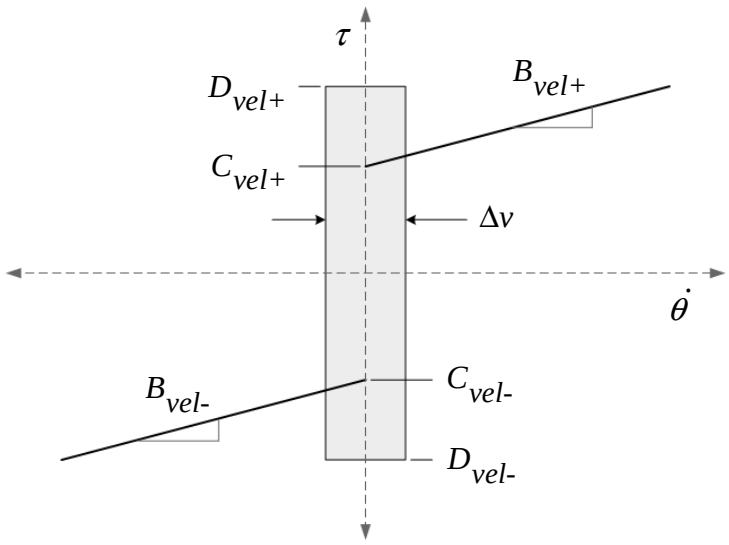

Figure 2: Karnopp Friction Model

Figure 3 illustrates a general detent model. A_{pos} represents the amplitude of a detent. Each crossing of the sinusoid across the x-axis represents a 'groove' or 'valley' of one detent. Consequently, P_{pos} changes the frequency of the detent. S_{pos} will shift the position of the detents along the knob.

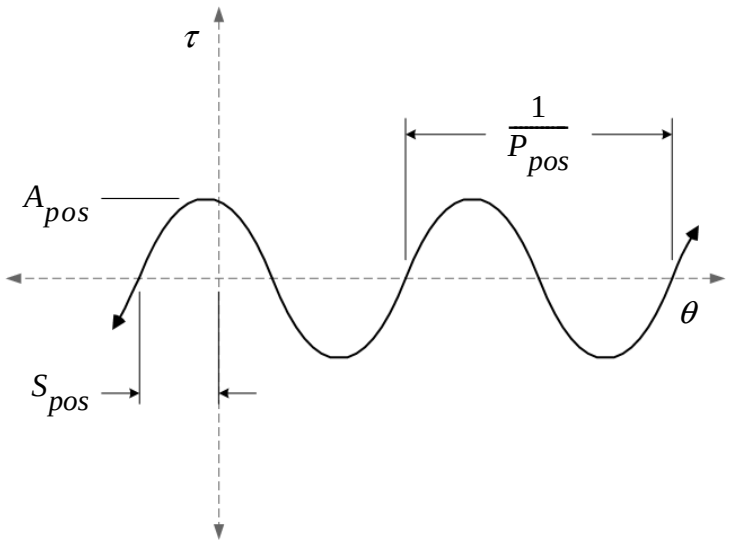

Figure 3: Detent Position Model

2.1 Some Previous Characterization Work

This characterization method is an extension and combination of several previous efforts:

- Richard [8] characterized the friction properties of three surfaces by linearly sliding across each surface with a load cell. The velocity and acceleration parameters shown in Equation 1 were fit using a least-squares algorithm.
- MacLean [5] used a haptic interface to measure the non-linear stiffness of a momentary switch. Different regions of the switch were individually characterized using non-linear force versus position curves.
- Miller and Colgate [7] also characterized force versus displacement data. They used a wavelet network to characterize in the spatial frequency domain without the need to manually segment out different non-linear regions.
- Weir *et al* [10] took a very pragmatic approach of visualizing mechanical properties of switches using coloured plots of position, velocity,

and / or torques. Differences between switches were compared by looking at the same 2D or 3D ‘haptic profiles’.

- Feo [2] took the approach of modeling with a single chaotic dynamic system. Instead of testing physical mechanical systems, Feo tested periodic signals such as time series from a spoken vowels and electrocardiograms. The linear dynamic parts and non-linear static parts identified by Feo closely resemble the dynamic and static components in Equation 1.

2.2 Simulated Characterization

Effectiveness of the characterization procedure can be tested using simulated perfect and noisy data that would typically be captured by the haptic camera. One example characterization of simulated data is illustrated below. The steps taken to test the characterization were:

1. Generate some physically possible position, velocity, and acceleration vectors (i.e., θ , $\dot{\theta}$, and $\ddot{\theta}$) based on a swept sine waveform.
2. Choose some scalers for each of the position, velocity, and acceleration parameters (e.g., A_{pos} , B_{vel+} , and M_{acc} , respectively)1.
3. Generate a torque vector (i.e., τ) by applying the simulated position, velocity, and acceleration vectors into Equation 1. Simulated noise can then applied to the torque vector.
4. Input the torque, position, velocity, and acceleration vectors into the characterization routines, and fit the data using non-linear least-squares curve fitting to the parameters in Equation 1.
5. Compare the values of the raw and fit values of the parameters in Equation 1.

Details of the above steps are described below.

2.2.1 Step 1: Generating Test Spatial Data

Physically valid swept sine waveforms for position, velocity, and acceleration were generated using Equation 3. First and second derivatives were calculated from the position function, and were used for the velocity and acceleration values, respectively, to ensure a physically valid dataset.

$$\theta = c\sin\left[\frac{\pi}{b-a}\left(\frac{(b-a)\,t}{d}+a\right)^2 - a^2\right] \tag{3}$$

$$\dot{\theta} = 2c\cos\left[\frac{\pi^2}{d\,(b-a)}\left\{\left(\frac{(b-a)\,t}{d}+a\right)^2 - a^2\right\}\left(\frac{(b-a)\,t}{d}+a\right)\right]$$

$$\ddot{\theta} = -4c\sin\left[\frac{\pi^3}{d^2\,(b-a)}\left\{\left(\frac{(b-a)\,t}{d}+a\right)^2 - a^2\right\}\left(\frac{(b-a)\,t}{d}+a\right)\right] +$$
$$2c\cos\left[\frac{\pi^2}{d^2}\left\{\left(\frac{(b-a)\,t}{d}+a\right)^2 - a^2\right\}\right]$$

Equation 4 shows the parameters used for this simulation, and Figure 4 illustrates the three signals.

$$t_n = \frac{n}{5000},\ n = 1, 30000 \tag{4}$$
$$a = 0,\ b = 1.5,\ c = 1.0,\ d = 3.0$$

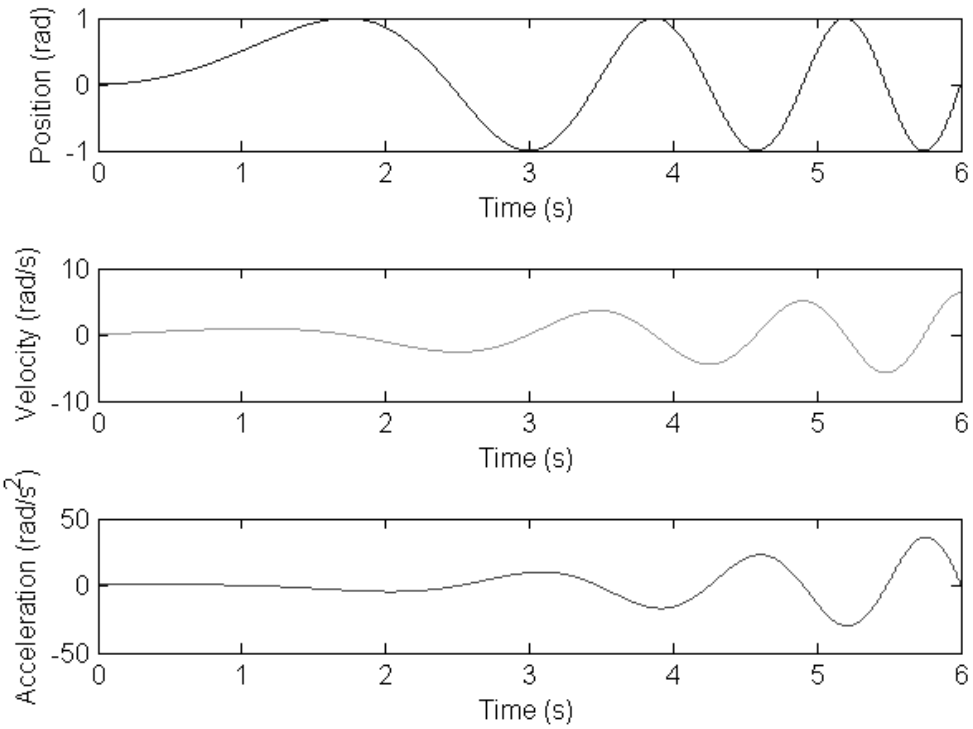

Figure 4: Simulated position, velocity, and acceleration curves

2.2.2 Step 2: Choosing Model Parameters

The position, velocity, and acceleration dependent parameters chosen for this simulation are shown below in Equation 5. Equation 5 is the same as Equation 1, but the symbolic scalers have been replaced numbers.

$$\tau = \begin{cases} 0.4\ddot{\theta} & \text{acc. part } (\tau_{acc}) \\ 1.5\,\mathrm{sgn}\,\dot{\theta}_{-} + 1.0\dot{\theta}_{-} + 2.0\,\mathrm{sgn}\,\dot{\theta}_{+} + 1.5\dot{\theta}_{+} & \text{vel. part } (\tau_{vel}) \\ 1.0\sin\left(\dfrac{\theta}{0.2} + 0.9\right) & \text{pos. part } (\tau_{pos}) \end{cases} \quad (5)$$

2.2.3 Step 3: Generating Test Torque Data

Simulated torques were then generated with Equation 5. A noisy torque signal was then generated using Equation 6.

$$\tau_{noisy} = \tau + 4.0(\text{rand}(\text{length}(\tau)) - 0.5) \quad (6)$$

where

length() = the number of torque values in τ.

rand() = a randomly selected number between 0 and 1 chosen from a Gaussian distribution.

The resulting torque signals with and without noise are shown in Figure 5.

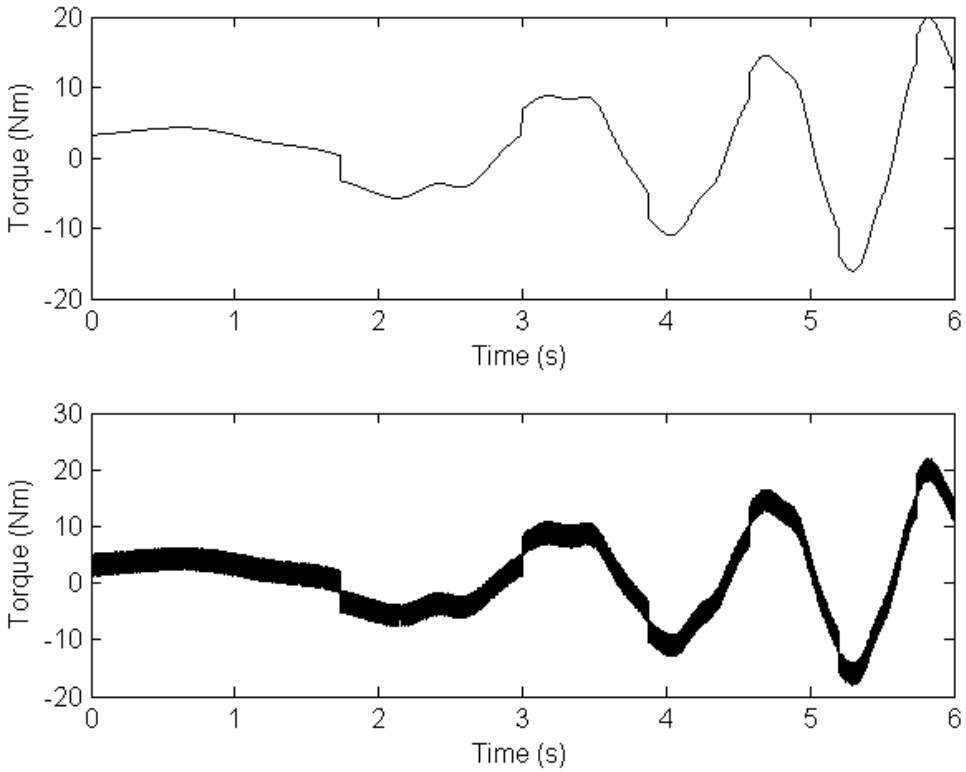

Figure 5: Simulated torques without (top) and with (bottom) noise

2.2.4 Step 4: Fitting to the Test Data

The spatial data shown in Figure 4 and the torque data shown in Figure 5 were then fit using the previously described separated non-linear least-squares curve procedure. Using the torque signal with no noise, a perfect

fit of the parameters was found after 7 iterations and 43 function counts with the Levenberg-Marquardt algorithm. With the noisy data, after 7 iterations and 46 function evaluations, the parameter fits were found as shown in Table 2.

Table 2: Fit Results for noisy simulated data

Param	M_{acc}	C_{vel-}	B_{vel-}	C_{vel+}	B_{vel+}	A_{pos}	P_{pos}	S_{pos}
Target	0.4	1.5	1.0	2.0	1.5	1.0	0.2	0.9
Fit	0.398	1.512	0.999	1.992	1.500	1.008	0.199	0.884

2.2.5 Step 5: Comparing Theoretical and Fit Data

Intuitively, the fit values shown in Table 2 closely match the theoretical values. Figures 6, 7, and 8 illustrate these results. The top plot of Figure 6 shows the overall fit torque vs. position and 95% confidence interval data superimposed on top of the raw torque data. The bottom of Figure 9 shows the data of just the position part (see Equation 5). Figure 7 shows the torque vs. velocity equivalents of Figure 6. The quality of the fit can be better seen by zooming into regions of the adjusted torque vs. position, and torque vs. velocity plots, as shown in Figure 8. These good fit results for noisy simulated data suggest that this characterization procedure should work reasonably well for data obtained from the haptic camera.

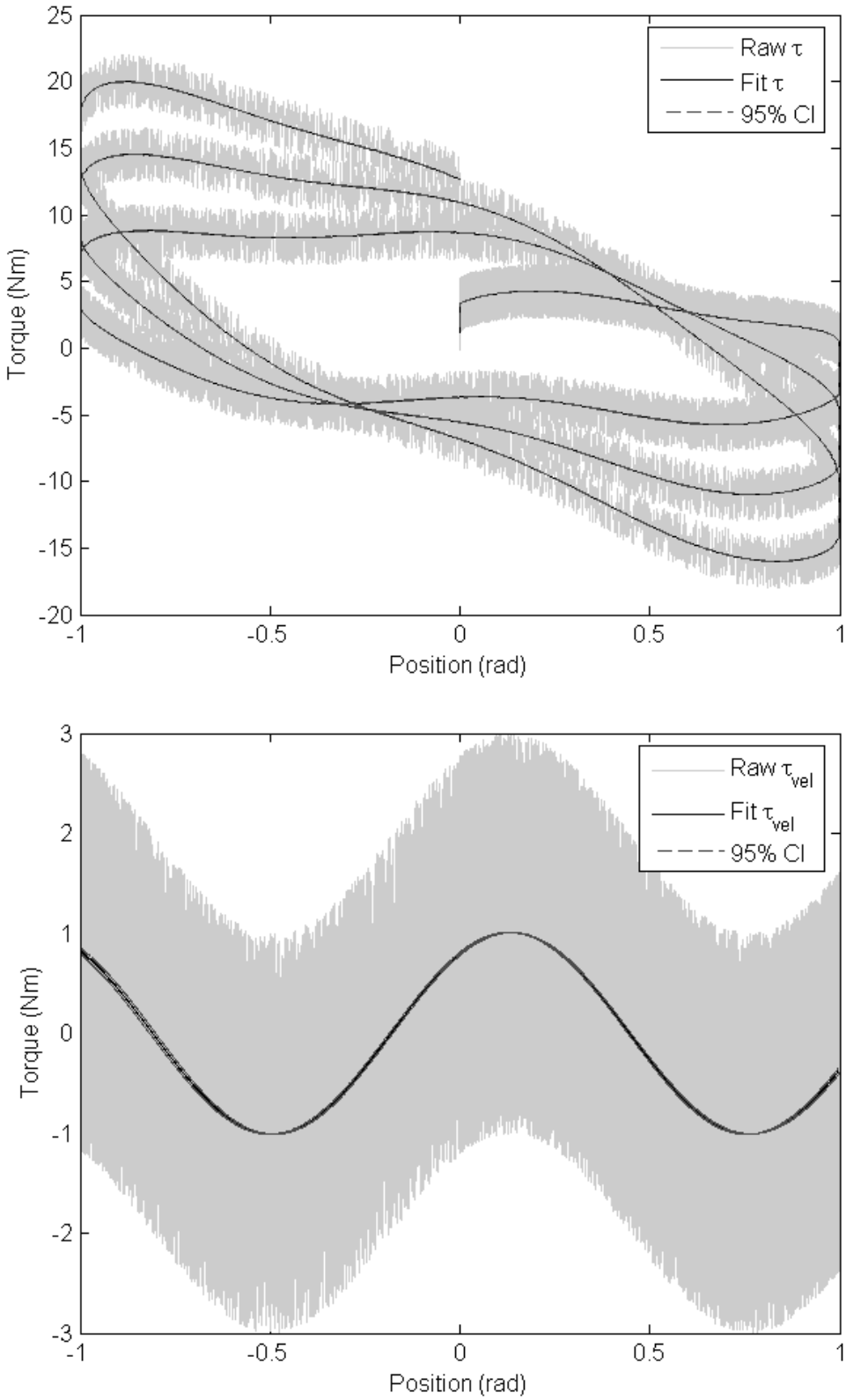

Figure 6: Fit torque vs. position plots for velocity & acceleration components

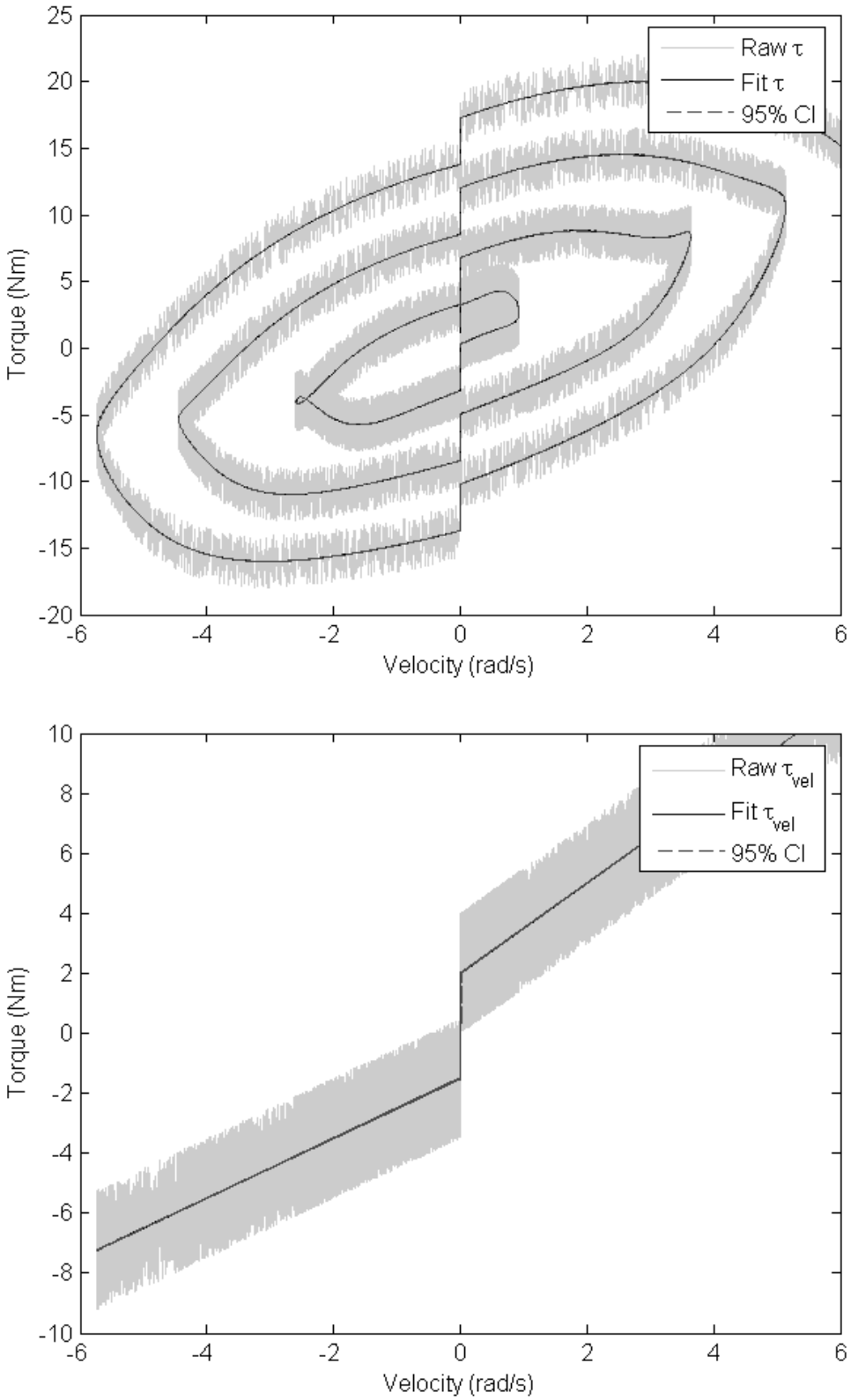

Figure 7: Fit torque vs. velocity plots without for position & acceleration components

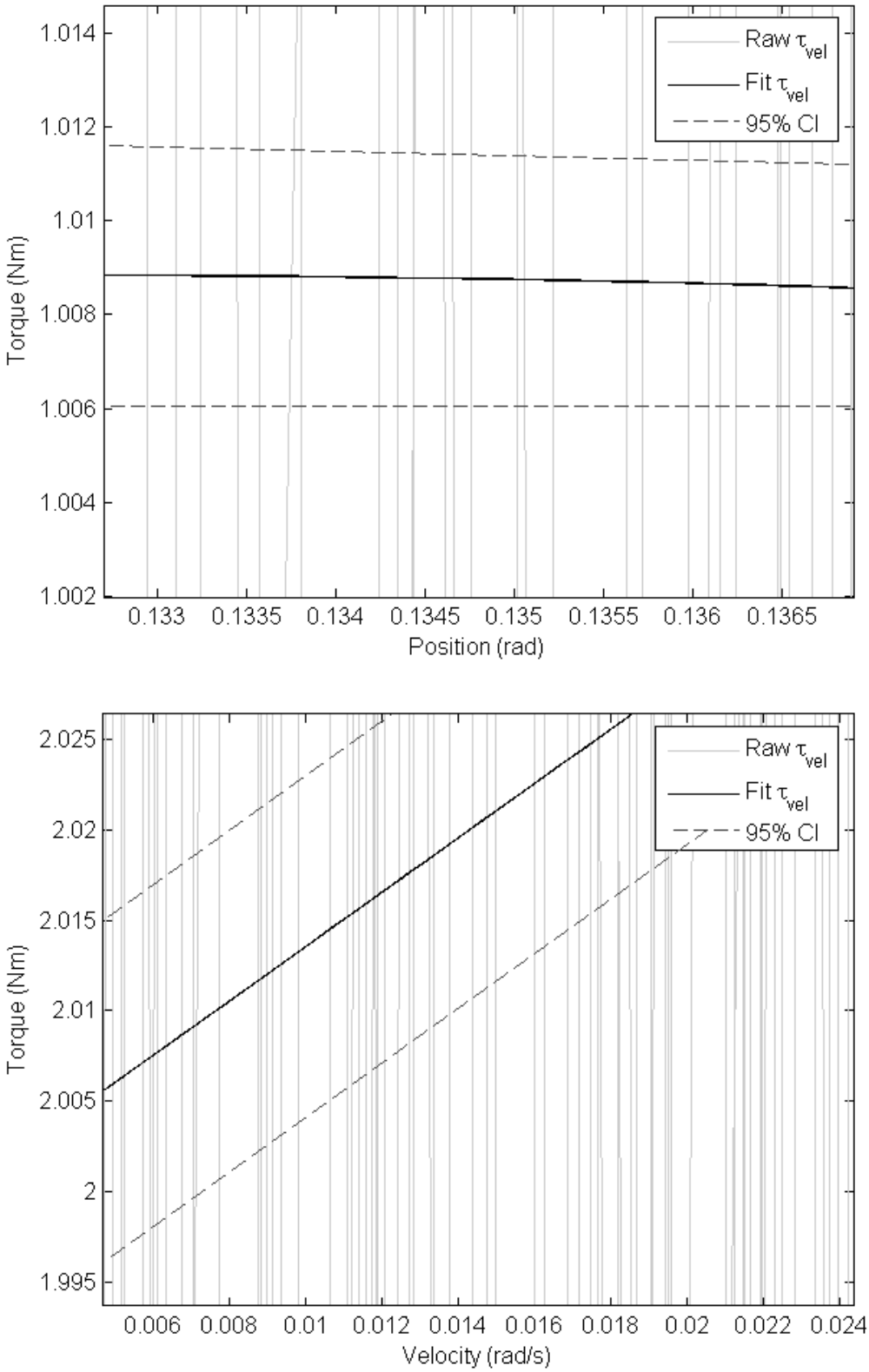

Figure 8: Zooms of adjusted torque vs. position (top) and torque vs. velocity plots (bottom)

3 Characterizing Real Knobs

We chose 5 mechanical knobs spanning a wide range of position, velocity, and acceleration dependent mechanical properties. The current haptic camera is designed for knobs that provide reaction torques between 0 - 200 mNm. Most consumer electronics, such as automobile consoles and household appliances, contain knobs with torque profiles within this range. Calibration of the haptic camera, and characterization of 5 mechanical knobs are described in the following section.

3.1 Sensor testing

A spatial and torque test were performed to test and calibrate the position, velocity, acceleration, and torque measurement capabilities. The basic idea with these tests was to command a signal according to a theoretical model, then compare the actual recorded results to the theoretical model. Rotary position was commanded for both tests using a swept sine, as previously shown in Equation 3. Tests were run for a 5 second interval while operating at a 5000 Hz update rate (i.e., over a set of 25 000 contiguous data points). Three independent executions were performed using the swept sine constants listed in Table 3.

Table 3: Swept sine constants for sensor tests

Test	*a*	*b*	*c*	*d*
Spatial	0.0	1.5	1.0	3.0
Torque	0.0	1.5	0.02	3.0

3.1.1 Spatial testing

Figure 9 illustrates a commanded position, velocity, and acceleration (wide grey lines) set of results using the haptic camera without an attached gripper. In other words, the motor could spin freely. Measured results (thin overlaid lines) closely followed the commanded position and velocity values. Acceleration values were also good after fitting using a least-squares algo-

rithm to a constant, C_{cal}, as shown in Equation 7. Three independent accelerometer calibrations were performed to estimate C_{cal} as ($\bar{x}$=1148, σ^2=117).

$$\ddot{\theta}_t = C_{cal}\ddot{\theta}_r \tag{7}$$

where

$\ddot{\theta}_t$ = calibrated acceleration in rad / s^2.

C_{cal} = 1148 (rad / s^2) / V conversion constant.

$\ddot{\theta}_r$ = raw acceleration from the haptic camera in volts.

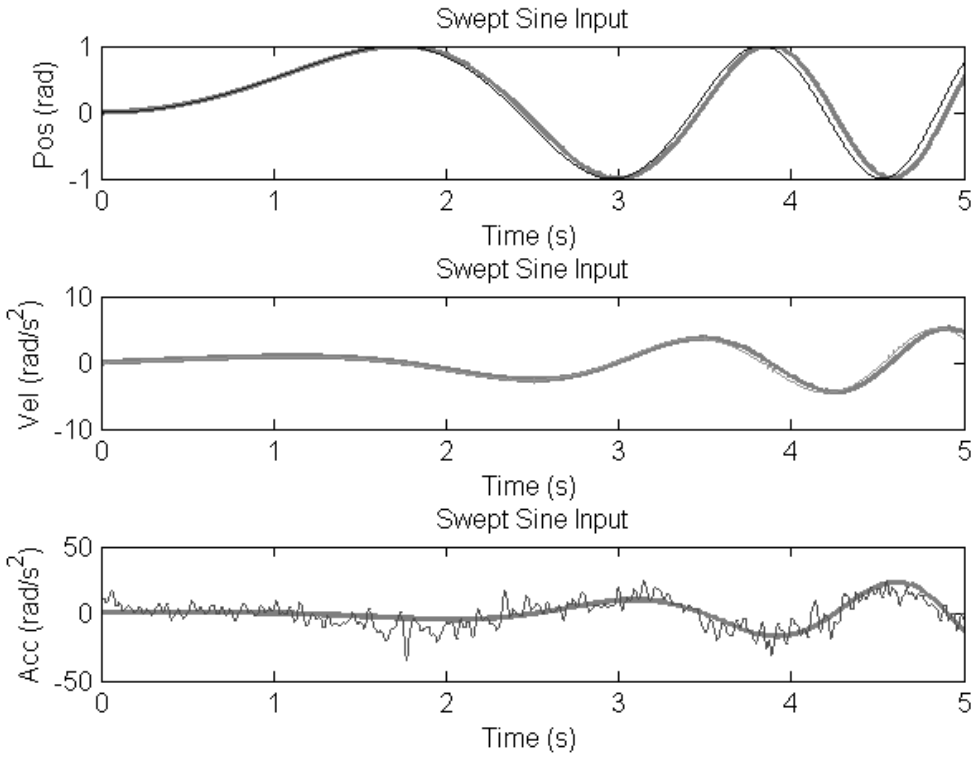

Figure 9: Theoretical and measured position (top), velocity (middle), and acceleration (bottom) values from a commanded swept sine signal

3.1.2 Torque testing

To test torque measurement ability, the haptic camera gripper was anchored to prevent any movement, and a small positional swept sine was

commanded. Figure 10 illustrates a theoretical (wide grey line) and measured torque (thin overlaid line) signal.

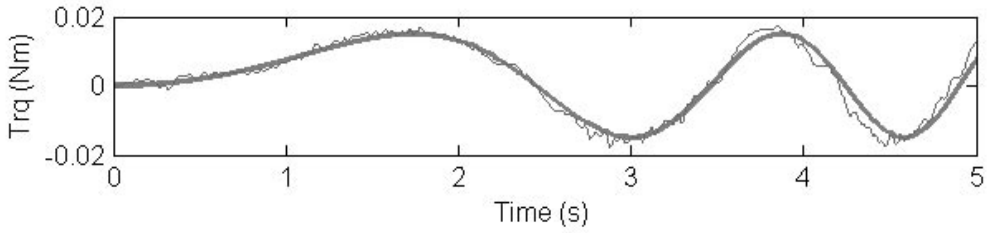

Figure 10: Theoretical and measured torque from a commanded swept sine signal

3.1.3 Test results

Standard deviations of the difference between the theoretical and recorded values are listed in Table 4. These results include a slight phase lag of < 1% after 25 000 updates that can be seen in Figures 9 & 10.

Table 4: Standard deviations of spatial and torque differences between theoretical and recorded signals

θ	$\dot{\theta}$	$\ddot{\theta}$	τ
0.0032 rad	0.0244 rad / s	0.4148 rad / s^2	0.0018 Nm

3.2 Capture of 5 knobs

Two captures for each of 5 mechanical knobs were performed. The first two knobs were uniform across position, whereas the last three knobs had detents. Thus, knobs 1 & 2 were primarily chosen to explore velocity and acceleration effects; whereas, knobs 3, 4, and 5 were primarily chosen to explore positional effects. Knob 5 was chosen as a 'worst case' fit since it has a large amount of backlash and very noticeable velocity non-linearities along different regions of the detents (i.e., violates our Lur'e system assumption). Knob numbers and their intuitive descriptions are listed in Table 5.

Table 5: Intuitive descriptions for 5 mechanical test knobs

Knob	Description
1	Uniform position; moderate friction; low inertia
2	Uniform position; low friction; high inertia
3	Very subtle, consistent detents; low friction; low inertia
4	Moderate, consistent detents; moderate friction; low inertia
5	Wide inconsistent detents & backlash; moderate friction; low inertia

3.2.1 Data preparation

Before fitting, the data was sorted by position and passed through a low pass filter to remove high-frequency noise. Pre-sorting by position is not detailed here because it is the same as previous characterization research such as Richard *et al* [8] and Colton & Hollerbach [1]. Third order Chebyshev type II IIR low pass filters with a stop band ripple of 20 dB were applied with the edge frequencies listed in Table 6. Phase shifts in the filtered data were avoided by filtering in two stages —once using forward filtering and once using backward filtering.

Table 6: Low pass filter stopband edge frequencies

θ	$\dot{\theta}$	$\ddot{\theta}$	τ
1000 Hz	1000 Hz	500 Hz	500 Hz

3.2.2 Data results

Table 7 lists the fit position, velocity, and acceleration parameters for two independent characterizations of each test knob.

Table 7: Two independent sets of fit parameters for knobs 1 - 5

Parameter	Knob 1	Knob 2	Knob 3	Knob 4	Knob 5
M_{acc}	0.069	0.28	0.034	0.049	-0.0048
$(mNm/rad/s^2)$	0.091	0.27	0.035	0.048	0.0085
C_{vel-}	-50	-3.8	-2.2	1.1	35
$(mNm/rad/s)$	-42	-13	-2.3	0.12	-3.5
B_{vel-}	1.8	-0.56	-0.16	0.48	6.4
$(mNm/rad/s)$	3.5	0.37	-0.14	0.62	2.9
C_{vel+}	50	3.8	2.2	1.1	35
$(mNm/rad/s)$	42	13	2.3	0.12	-3.5
B_{vel+}	-7.5	0.47	-0.25	0.56	6.7
$(mNm/rad/s)$	-1.5	0.61	-0.23	-0.0062	1.4
D_{vel-}	-150	-17	-10	-20	-200
(mNm)					
D_{vel+}	150	17	10	20	200
(mNm)					
Δv	0.040	0.015	0.010	0.010	0.015
(mNm)					
A_{pos}			1.2	-11	-202
(mNm)			0.97	-11	-61
P_{pos}			0.034	0.076	0.16
(1)			0.035	0.076	0.041
S_{pos}			0.00046	-0.19	-0.16
(rad)			0.17	-0.22	-1.9
95% CI	0.26	0.18	0.098	0.073	3.3
(mNm)	0.35	0.20	0.084	0.072	5.1

Figures 11 - 23 illustrate captured torque vs. position and torque vs. velocity data that highlight the detent and friction components of the five knobs, respectively. Torque vs. acceleration plots are not shown because only one acceleration variable, M_{acc}, was 'fit' with the capture model. These plot legends show five different types of data:

- ***Raw*** τ: Raw torque values from the torque sensor after being low-pass filtered (See "Data preparation" on page 17.).
- ***Fit*** τ: torque result from Equation 1 using measured position, velocity, and acceleration with fit values of position, velocity, and acceleration parameters such as S_{pos}, B_{vel+}, and M_{acc}, respectively.
- ***Raw*** τ_{pos} & τ_{vel}: raw torque values after subtracting non-position or non-velocity components from the torque vs. position or torque vs. velocity plots, respectively. For example, 'clean' the detents (primarily position related) and inertia (primarily acceleration related) from torque vs. velocity plot to isolate out friction components (primarily velocity related).
- ***Fit*** τ_{pos} & τ_{vel}: torque result from Equations 2 and 3 *without* using measured values of position, velocity, or acceleration. Only the position or velocity parts of Equations 2 and 3 were plotted for the torque vs. position or torque vs. velocity plots, respectively.
- ***95% CI***: 95% confidence interval (e.g., *nlpredci* command in Matlab) for the presented data.

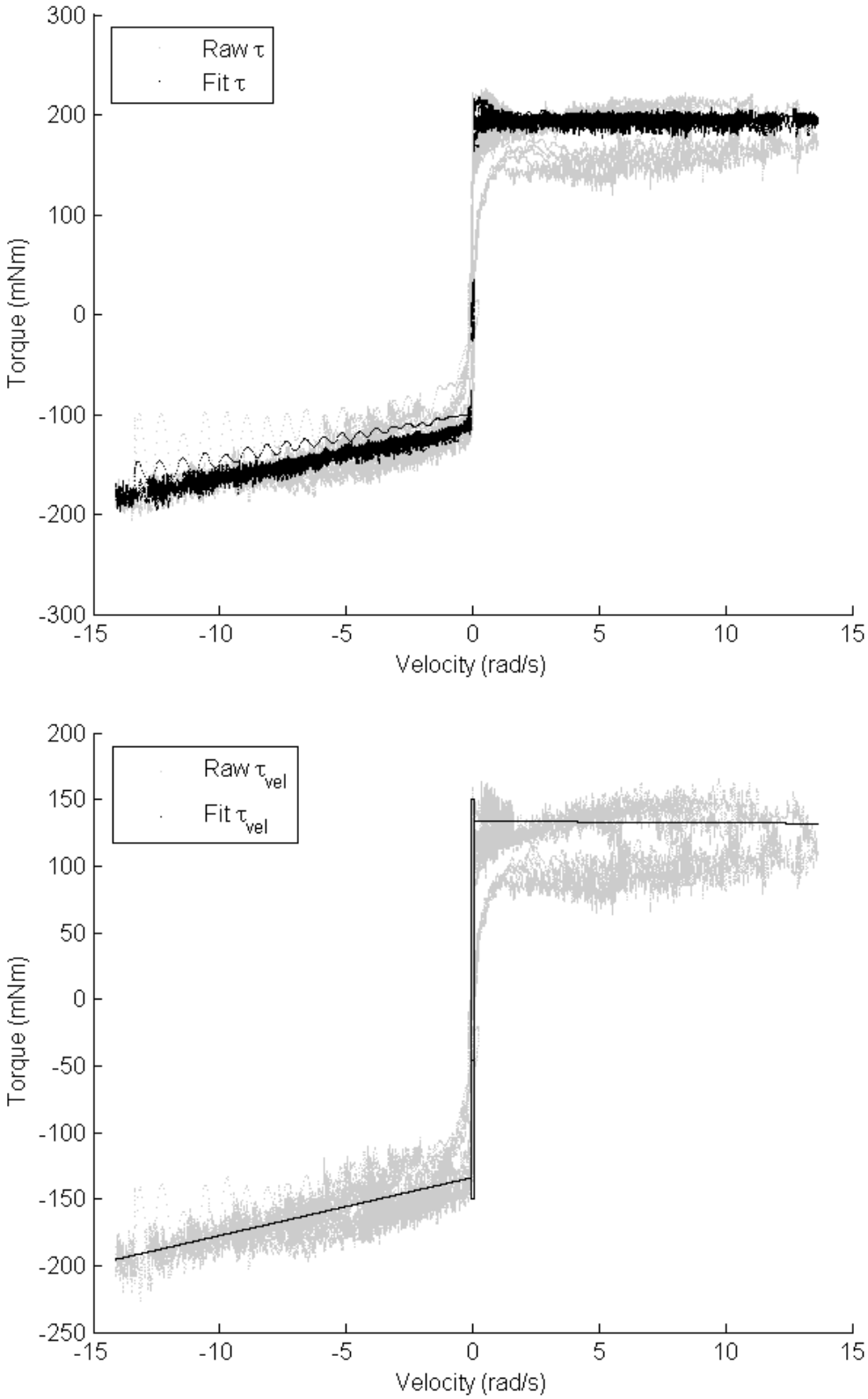

Figure 11: Torque vs. velocity plots for knob 1

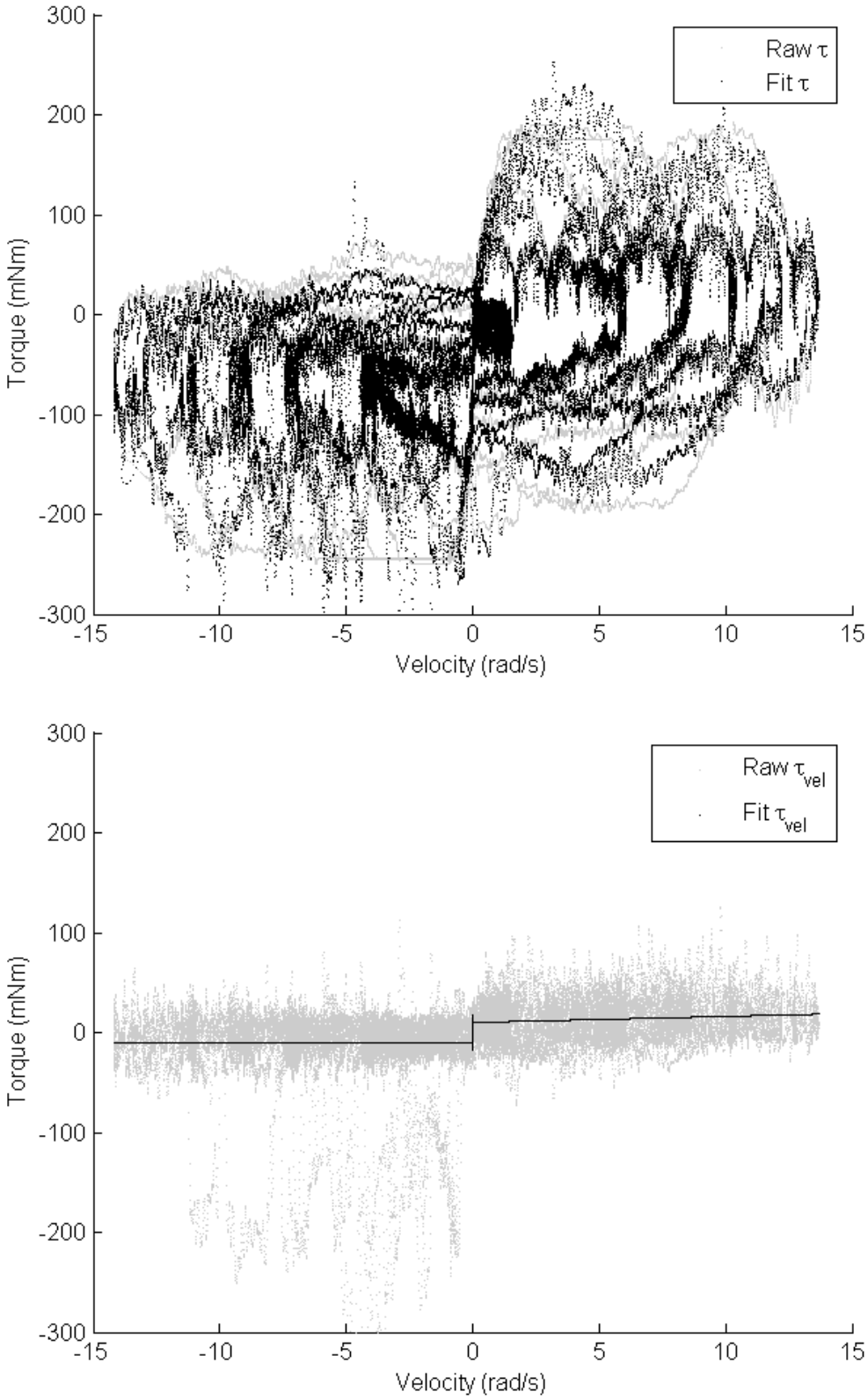

Figure 12: Torque vs. velocity plots for knob 2

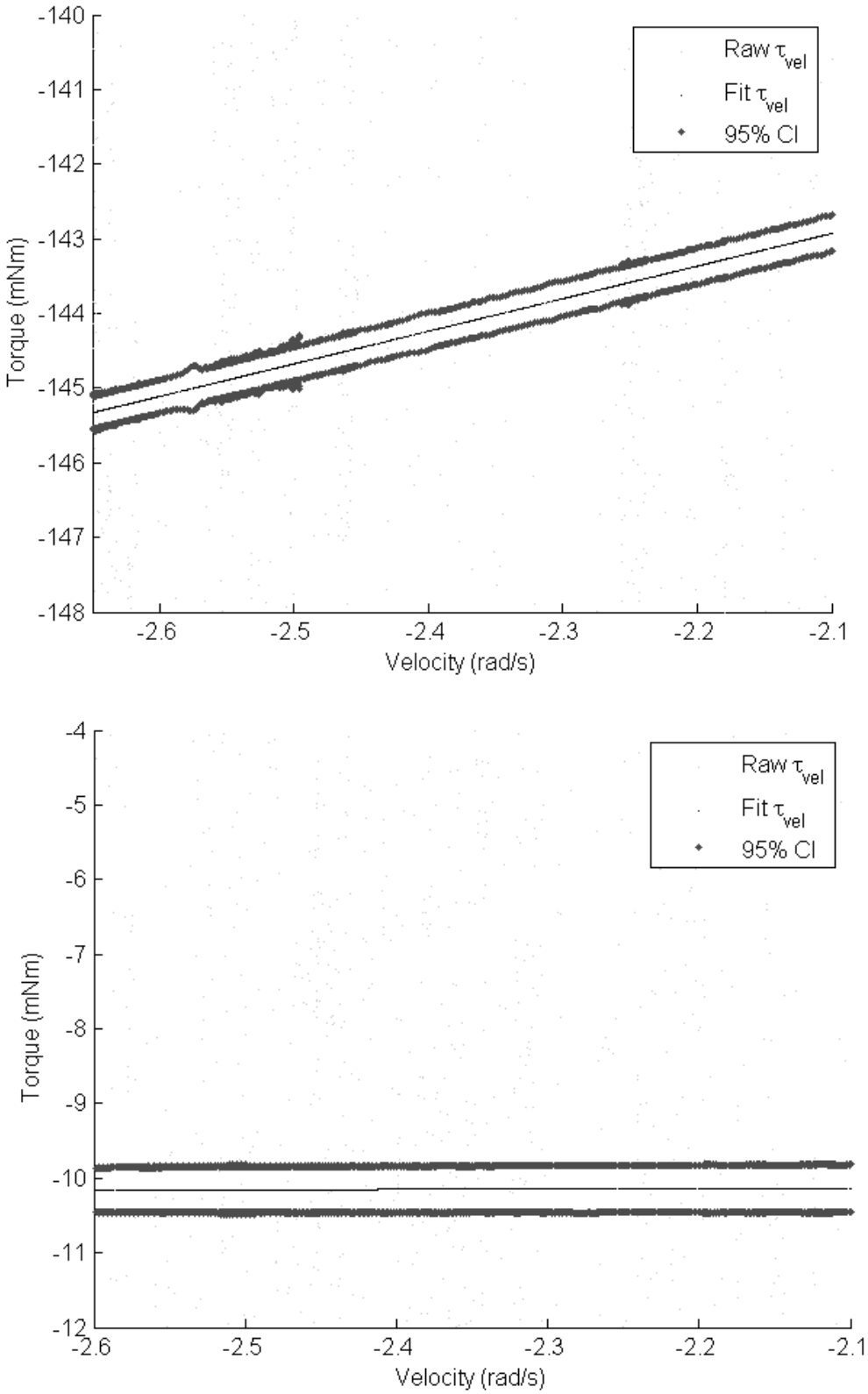

Figure 13: Zooms of torque vs. velocity plots for knob 1 (top) and knob 2 (bottom)

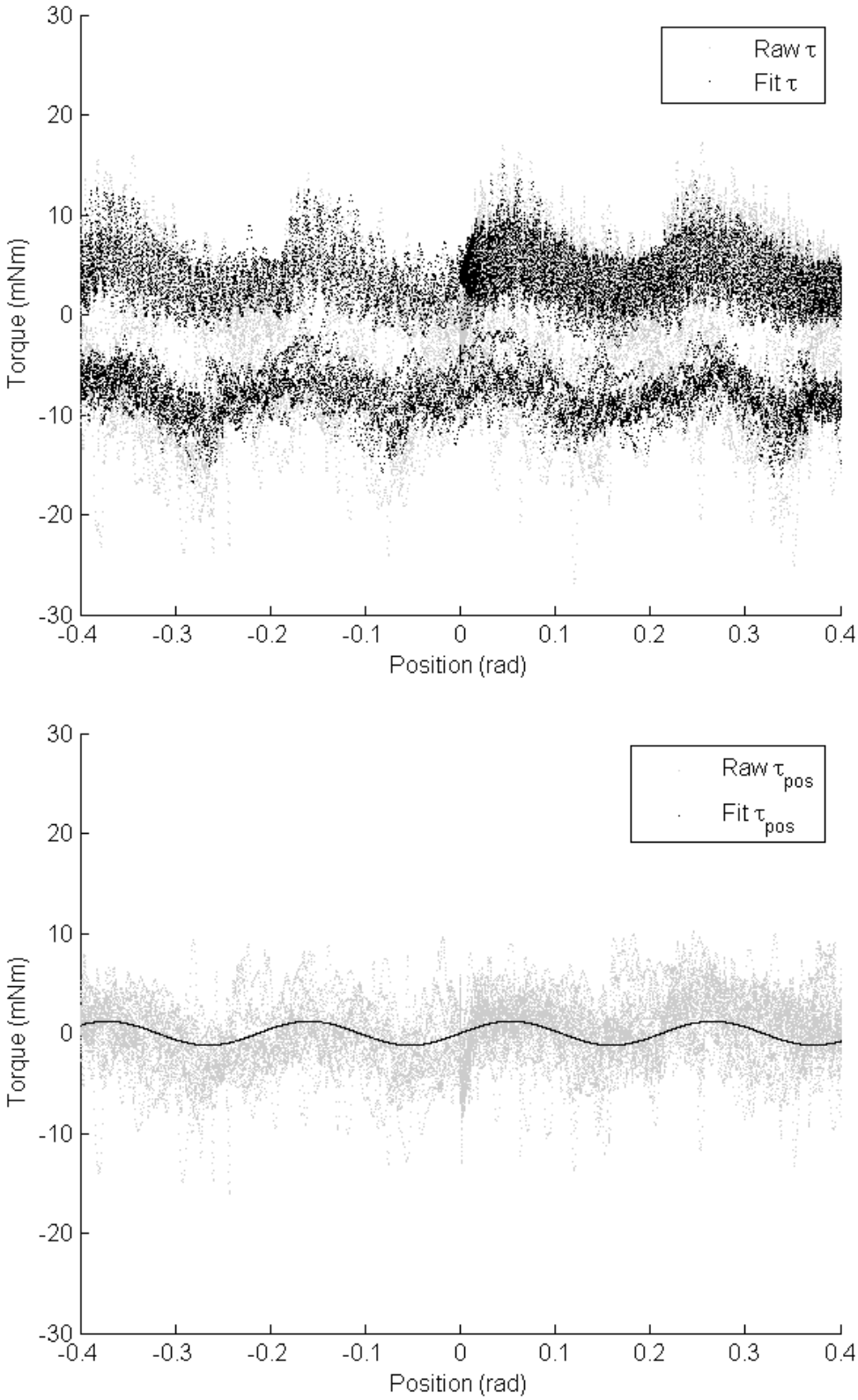

Figure 14: Torque vs. position plots for knob 3

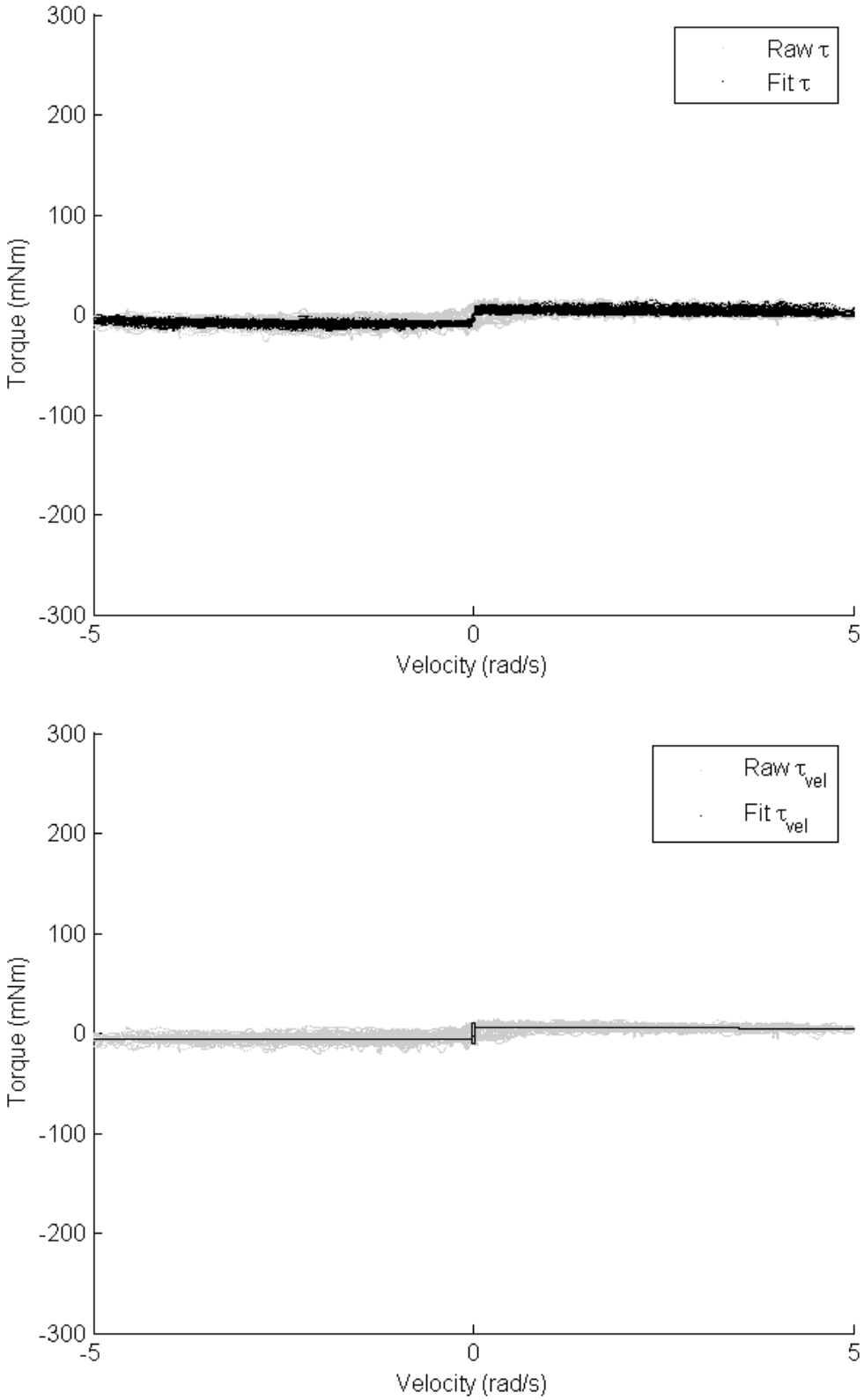

Figure 15: Torque vs. velocity plots for knob 3

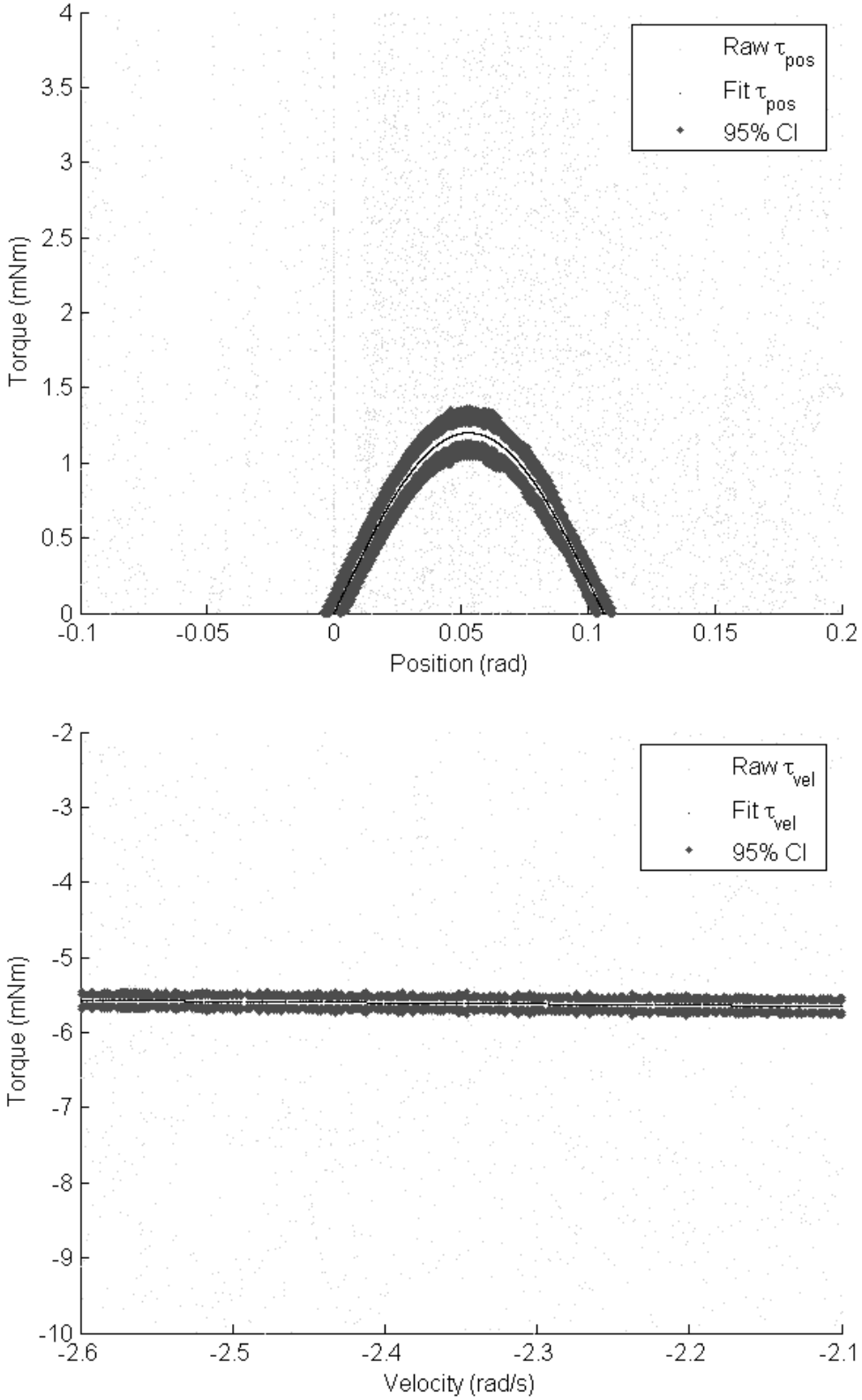

igure 16: Zooms of torque vs. position (top) torque vs. velocity plots (top) for knob 3

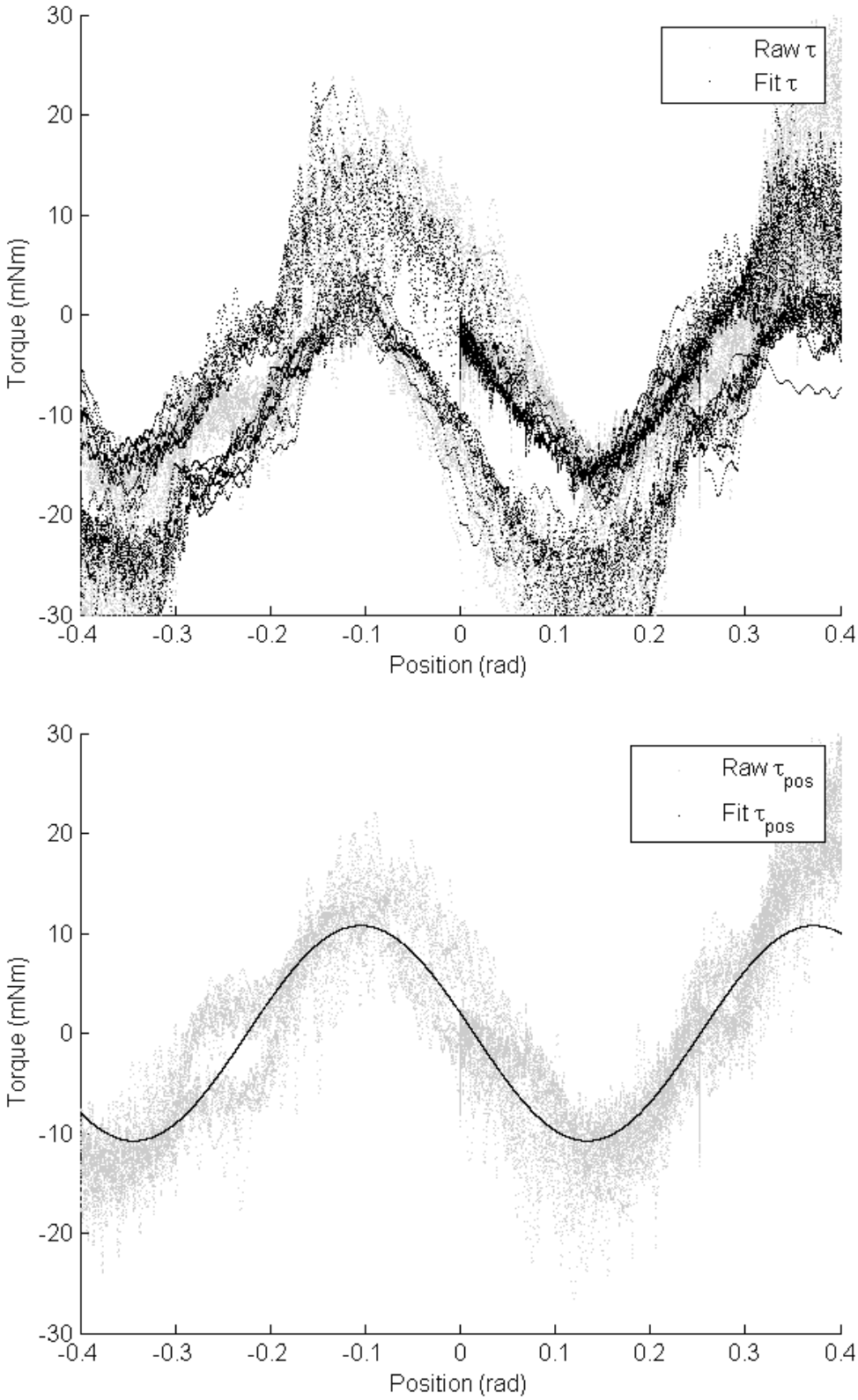

Figure 17: Torque vs. position plots for knob 4

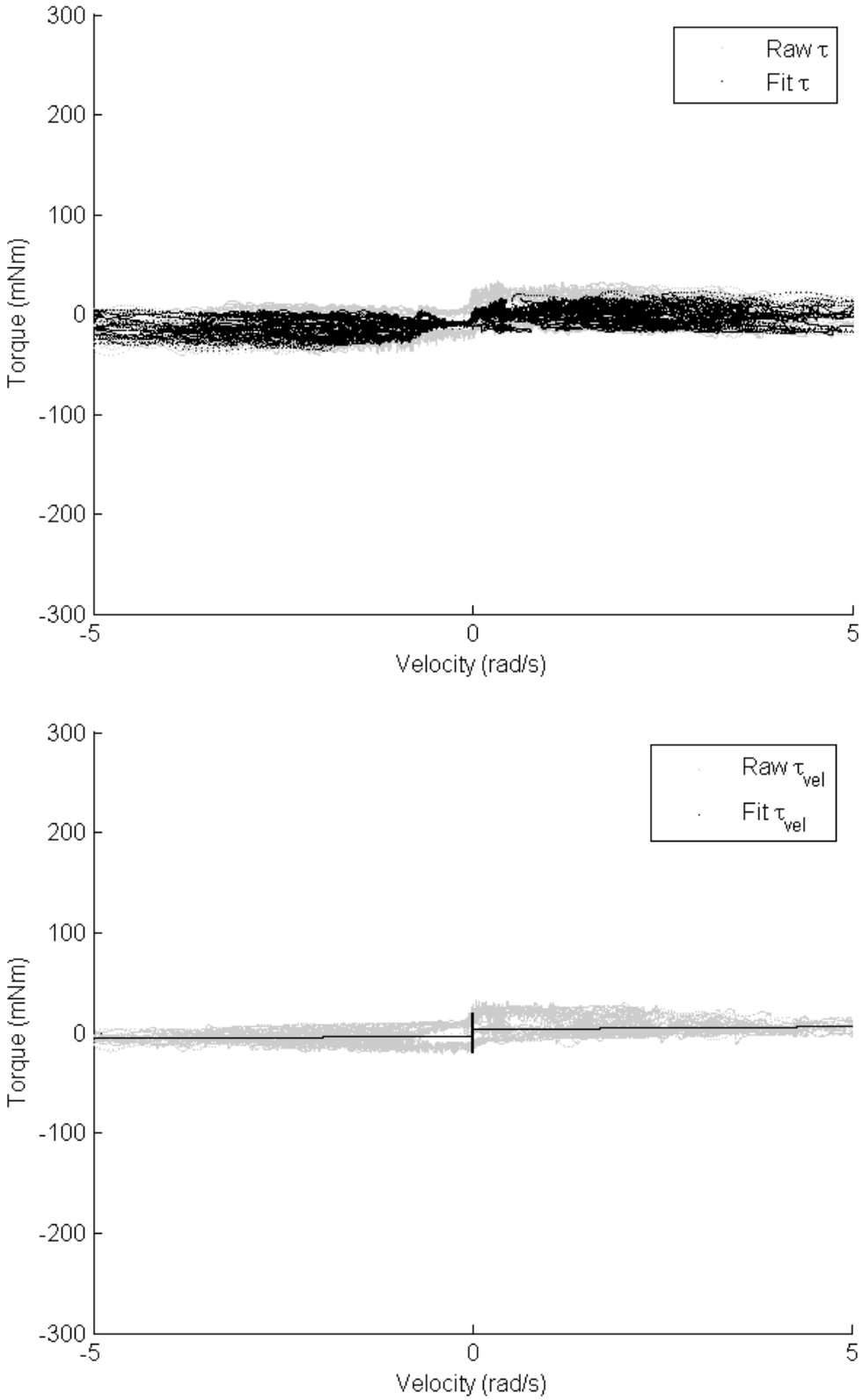

Figure 18: Torque vs. velocity plots for knob 4

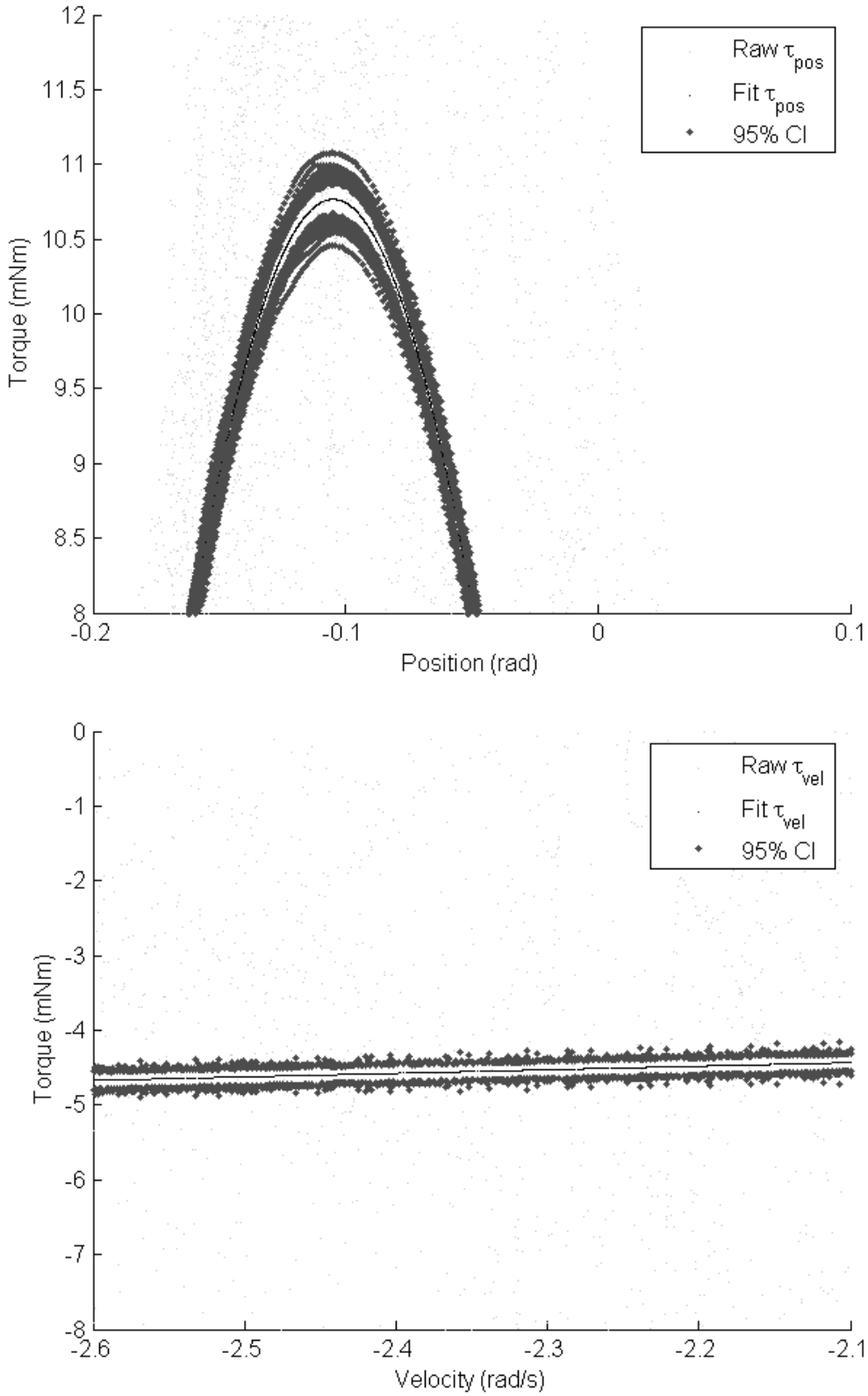

igure 19: Zooms of torque vs. position (top) torque vs. velocity plots (top) for knob 4

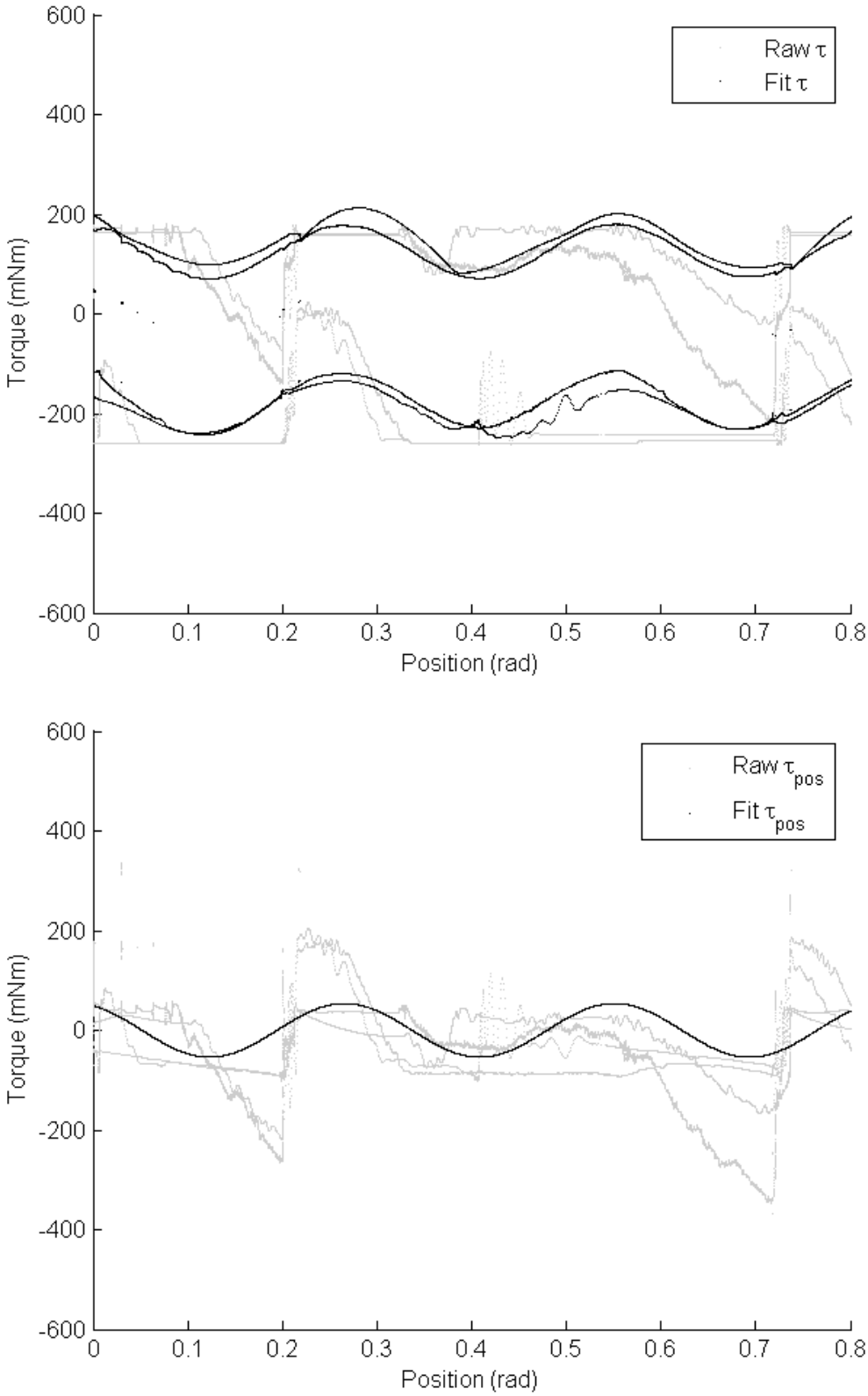

Figure 20: Poor matches of torque vs. position plots for knob 5

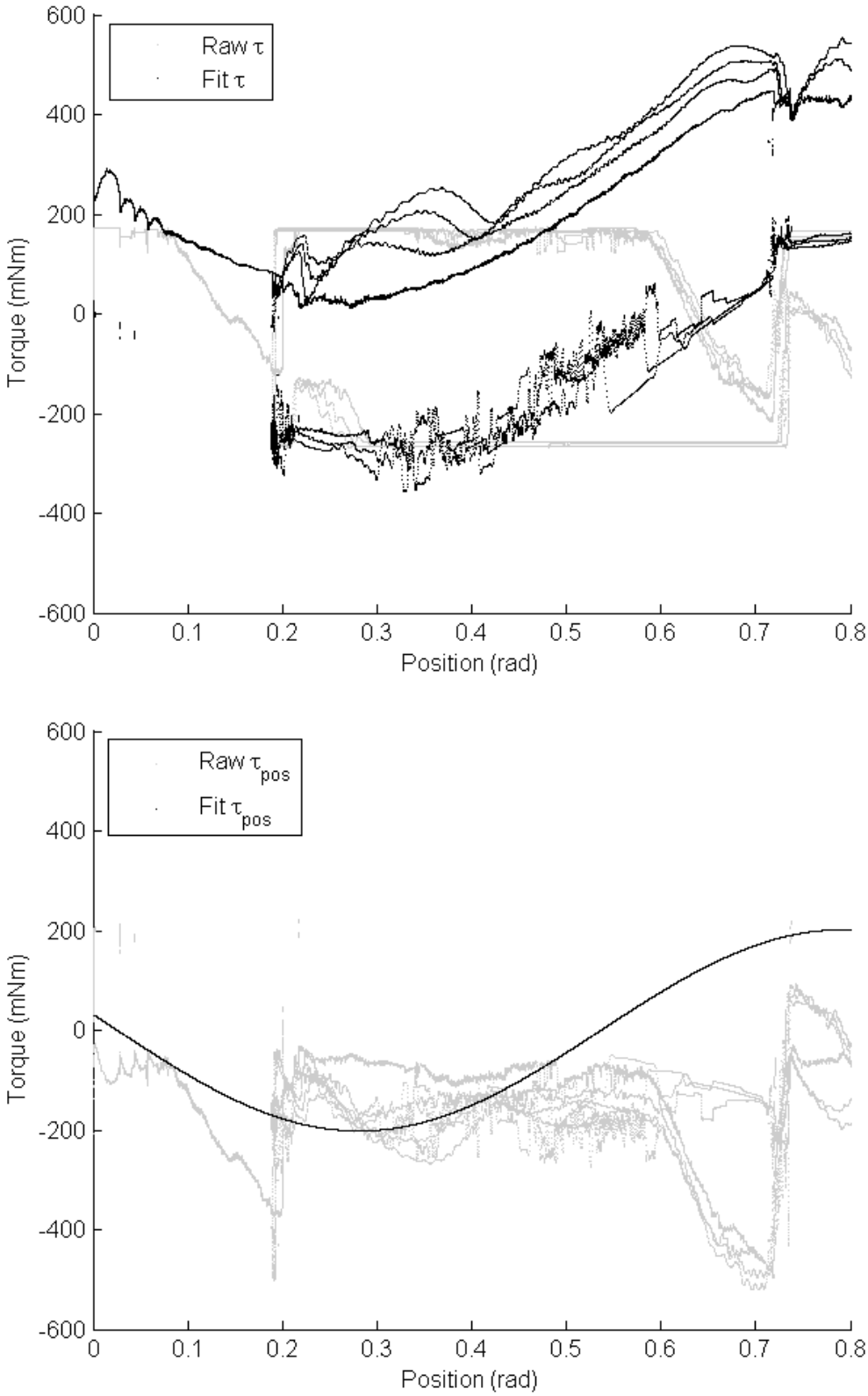

Figure 21: Acceptable matches of torque vs. position plots for knob 5

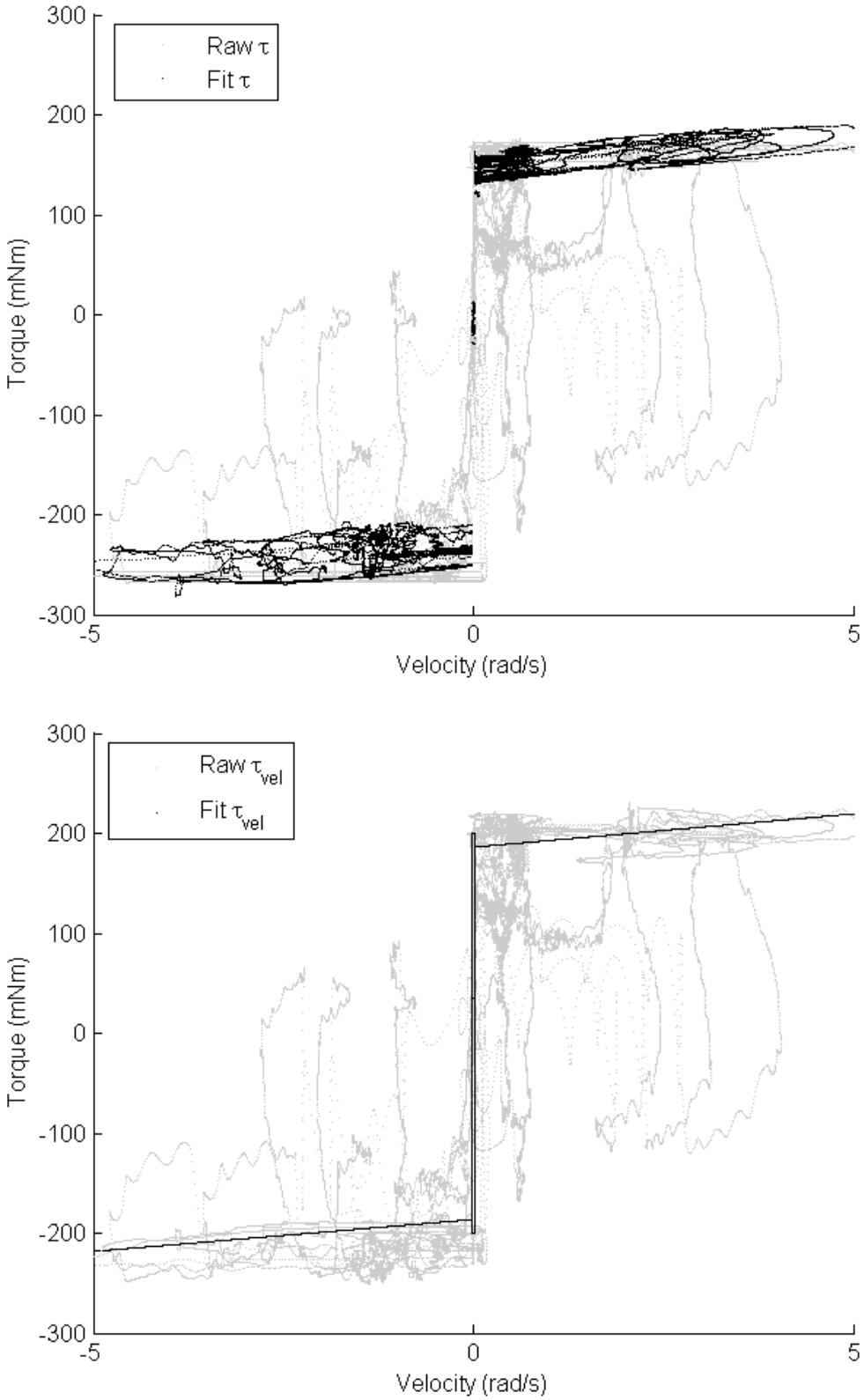

Figure 22: Torque vs. velocity plots for knob 5

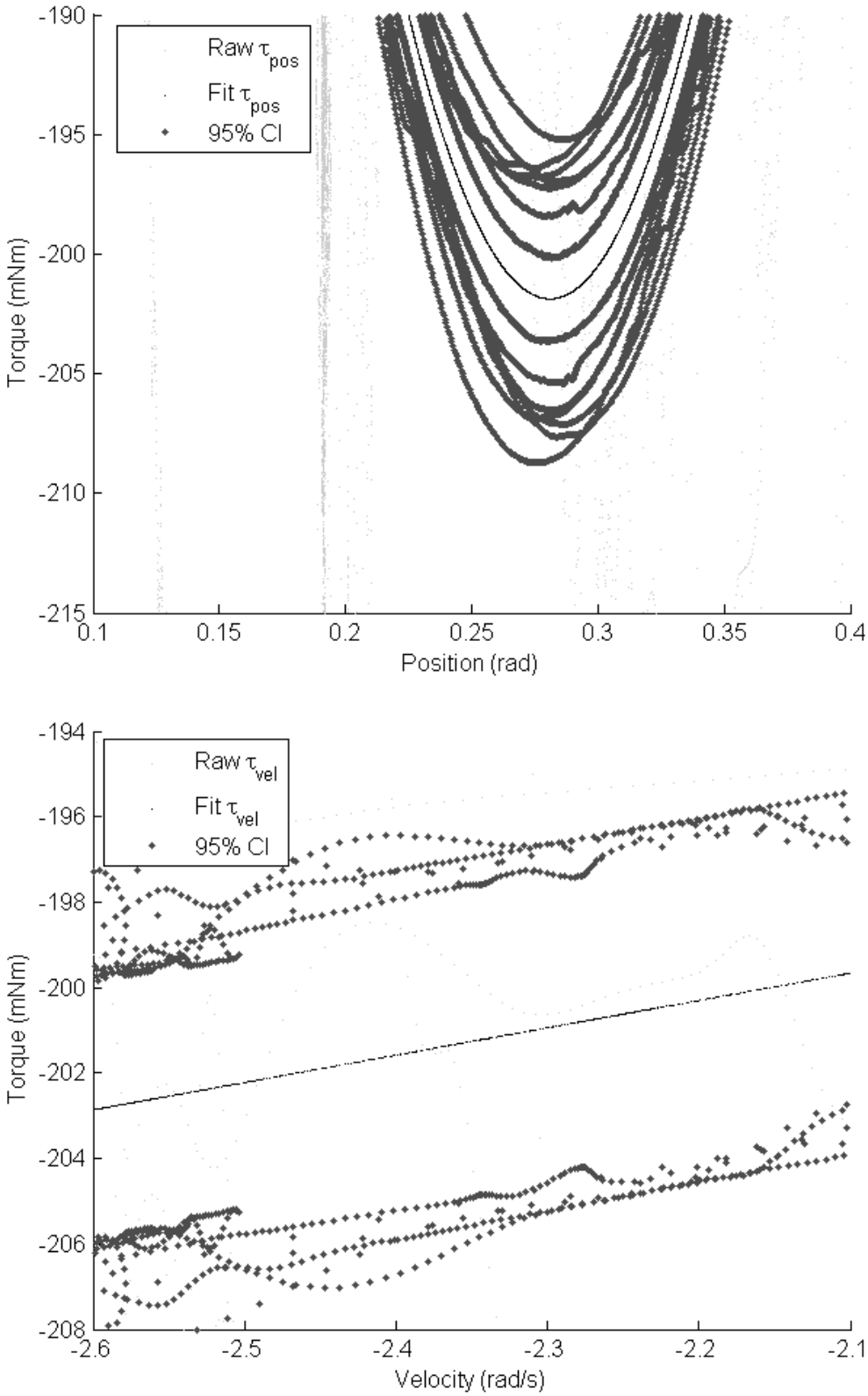

igure 23: Zooms of torque vs. position (top) torque vs. velocity plots (top) for knob 5

3.2.3 Summary

Analyses of the captured data are summarized in Table 8. Since knobs 1-2 were spatially uniform and knobs 3-5 had detents,

Table 8: Summary of Knob Characterization Plots

Knob	Description
1	The top and bottom plots of Figure 11 have a clearly defined form similar to the Karnopp friction model. Capturing dynamics were expected to be easier for this knob than the other knobs because the feel of knob 1 had no detents or high inertia components, and had a uniform, moderate friction. The 'loop' of '*Raw* τ_{vel} ' data at the top right of Figure 11 (bottom) suggests a small amount of variance from the fit model (i.e., Equation 1). Figure 13 shows 95% CI torque values < 1 mNm for torques with magnitudes > 140 mNm, indicating a successful fit.
2	The higher inertia and subtle friction of knob 2 made fitting more difficult than knob 1. Consequently, a much greater difference can be seen between the '*Raw* τ' and '*Raw* τ_{vel}' data in Figure 12 compared to Figure 11. Nevertheless, Figure 12 highlights very good separation of velocity and acceleration effects. Acceleration torque effects of magnitudes ~200 mNm completely dominate the velocity effects in the top of Figure 12. But, the bottom of Figure 12 shows relatively clean separation of small ~20 mNm velocity effects from the dominating acceleration effects. A small amount of improperly fit data can be seen at the bottom left of Figure 12. This region of '*Raw* τ_{vel}' torque data was probably caused by saturation of the torque sensor during the captures because the torque sensor and data acquisition hardware were only rated to ±180 mNm. Like knob 1, Figure 13 the 95% CI suggest a successful fit.
3	The double 'ghosted' '*Raw* τ' and '*Fit* τ' data at the top of Figure 14 were due to velocity and acceleration effects. The expected sinusoid for a knob with detents is clearly visible at the top of Figure 14, and well segmented into the '*Raw* τ_{pos}' and '*Fit* τ_{pos}' values at the bottom of Figure 14. The bottom plots of Figures 14 & 15 suggest that the very subtle ~10 mNm peak detents and friction were successfully fit. Additionally, the 95% CI plots of Figure 16 suggest a dominance of appropriate signal data over noisy data such as the 'salt and pepper' noise sprinkled throughout these plots.

Table 8: Summary of Knob Characterization Plots

Knob	Description
4	Figure 17 clearly shows the larger amplitude and lower frequency detents of knob 4. Comparing Figure 17 to Figure 18, we can see that the detents dominate the feel of knob 4. This domination contrasts with knob 3 where the detents and friction had similar contributions to the knob's feel. The bottom of Figure 18 is a considerable improvement over the top of Figure 18, but the ghosting present in this plot, and the bottom of Figure 17, suggest increased difficulty fitting these data compared to equivalent data for knob 4. Nevertheless, the fit was relatively successful, as suggested by the good 95% CI plots of Figure 19.
5	Figures 20 & 21 show the difficulty attempting to fit data to the Equation 1 model. For example, before performing a capture, casually turning knob 5 revealed significant backlash and non-sinusoidal detents. For example, physical slips due to the considerable backlash can be seen between 0.1 - 0.2 rad in Figures 20 & 21. These torque vs. position fits were also quite sensitive to subtle changes in the fitting procedure such as different initial conditions for the non-linear model parameters. Nevertheless, Figure 21 shows how the fitting procedure could 'see beyond' the backlash and fit a sine wave of appropriate frequency to the captured knob 5 data. As one would hope, these positional effects were successfully isolated from the velocity and acceleration effects. The torque vs. velocity plots in Figure 22 shows a good fit to the friction model parameters even though some aliasing can be seen in both the '*Raw* τ' and '*Raw* τ_{vel}' plots. Such aliasing was not present in comparable plots for knobs 1 - 4. As a further indication of difficult fit, the magnitudes of the 95% CIs from the fit torques in Figure 23 were more than 10 times greater than knobs 1 - 4. Overall, the modest success fitting knob 5 suggests a promising robustness to the fit procedure since the feeling of knob 5 so clearly deviated from the fit model of Equation 1.

Figure 29 gives a detailed zoom of torque vs. velocity data plot to show how the static friction parameters were estimated for each of the 5 knobs. The density of '*Raw* τ_{vel}' data points abruptly drop beyond ±0.01 rad to indicate the appropriate Δv boundary. Similarly, the densities for torque drop off beyond ±10 mNm to indicate the appropriate D_{vel-} and $_{vel+}$ boundaries;

although, in this example, the density drop-offs for the D_{vel} stick-slip boundaries were less clear than for Δv. Some noise is visible near ±10 mNm in Figure 29, but is virtually non-existent elsewhere in the plot. Overall, a clear match to the Karnopp friction model is evident for this example knob containing very subtle amounts of friction.

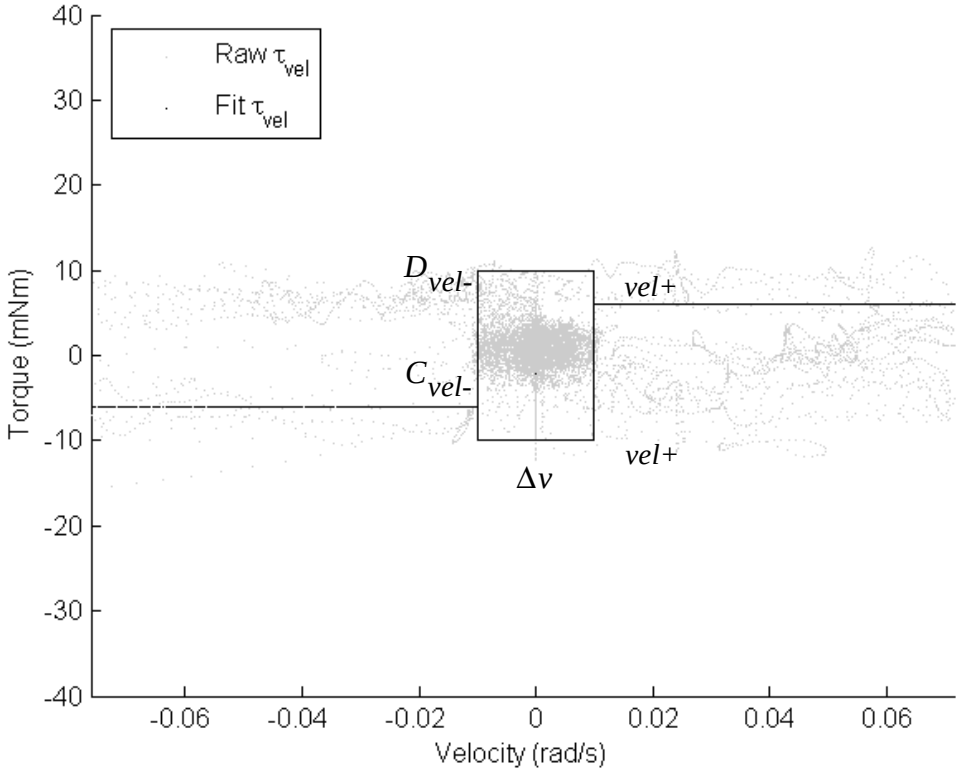

Figure 24: Example static friction parameter estimation on the torque vs. velocity data from knob 3

References

[1] Colton, M.B., & Hollerbach, J.M. (2005). Identification of Nonlinear Passive Devices for Haptic Simulations. In *Proc. of Haptic Interfaces for Virtual Environments and Teleoperator Systems (HAPTICS),* IEEE, 363 - 368.

[2] Feo, O.D. (2003). Self-emergence of chaos in the identification of irregular periodic behavior. *Chaos: An Interdisciplinary Journal of Nonlinear Science, 13*(4), 1205 - 1215.

[3] Gill, P.R., Murray, W., and Wright, M.H. (1981). *Practical Optimization*. Academic Press, 136 - 137.

[4] Karnopp, D. (1985). Computer simulation of stick-slip friction in mechanical dynamic systems. *Journal of Dynamic Systems, Measurement, and Control, 107,* ASME, 100 - 103.

[5] MacLean, K.M. (1996). The Haptic Camera: A Technique for Characterizing and Playing Back Haptic Properties of Real Environments. In *Proc. of Haptic Interfaces for Virtual Environments and Teleoperator Systems (HAPTICS),* ASME/IMECE, 459 - 467.

[6] Mathworks, Inc. (2005, July 19). *Solution Number: 1-18E03.* Available at: http://www.mathworks.com/support/solutions/data/1-18E03.html?product=OP&solution=1-18E03.

[7] Miller, B.E. and Colgate, J.E. (1998). Using a Wavelet Network to Characterize Real Environments for Haptic Display. In *Proc. of Dynamic Systems, and Control Division, DSC 58,* ASME, 257 - 264.

[8] Richard, C. (2000). *On The Identification and Haptic Display of Friction.* Ph.D. Thesis. Stanford University.

[9] Stribeck, R. (1902). Die wesentlichen Eigenschaften der Gleitund Rollenlarger [The key qualities of sliding and roller bearings]. *Z. Vereines Deutsch Ingen 46*(38,39), 1342-1348, 1432-1437.

[10] Weir, D.W., Peshkin, M., Colgate, J.E., Buttolo, P., Rankin, J., and Johnston, M. (2004). The Haptic Profile: Capturing the Feel of Switches. In *Proc. of Haptic Interfaces for Virtual Environments and Teleoperator Systems (HAPTICS),* ASME/IMECE.